Iron encapsulated carbon nanotube composites embedded in alumina with enhanced magnetic properties

Steven Rhodes [a], Warner Cribb [b], Valentin Taufour [c], Dwight Patterson [d], Dereje Seifu [e], Saeed Kamali [a,f,*], Suman Neupane [a,**]

[a] Department of Physics and Astronomy, Middle Tennessee State University, Murfreesboro, TN, United States
[b] Department of Geosciences, Middle Tennessee State University, Murfreesboro, TN, United States
[c] Department of Physics and Astronomy, University of California, Davis, CA, United States
[d] Department of Chemistry, Middle Tennessee State University, Murfreesboro, TN, United States
[e] Department of Physics and Engineering Physics, Morgan State University, Baltimore, MD, United States
[f] Department of Mechanical, Aerospace and Biomedical Engineering, University of Tennessee Space Institute, Tullahoma, TN, United States

ARTICLE INFO

ABSTRACT

Alumina is an essential ceramic insulator, while carbon nanotubes (CNTs) have intriguing mechanical, thermal, electrical, and magnetic properties. We report on the synthesis of CNTs/Al_2O_3 nanocomposites using the chemical vapor deposition (CVD) process using iron as a catalyst. The as-prepared composite's structure and morphology are characterized by transmission electron microscope, scanning electron microscope, X-ray diffractometer, thermogravimetric analyzer, and Mössbauer spectroscopy. The experimental results show that these composites contain CNTs of an average diameter of 40 nm distributed homogenously within the alumina matrix. The percentage of CNTs within the composites is at 7%. The CNT/Al_2O_3 nanocomposites demonstrate a dramatic enhancement of ferromagnetic properties during vibrating sample magnetization measurements. As compared to the magnetization of 0.03 e.m.u./g at an applied field of 1.5 T for the Fe-catalyzed Al_2O_3, the saturation magnetization of CNT/Al_2O_3 is 1.78 e.m.u./g, which represents an increment of ~5800%. The coercivity of CNTs/Al_2O_3 composites increased from 0.036 T at 300 K to 0.285 T at 5 K. This study provides a relatively simple approach to blending the magnetic properties with potential thermoelectric materials.

1. Introduction

Carbon nanotubes (CNTs) continue to excite researchers with their potential to develop nanostructures for applications in material science, medicine, and electronics [1–4]. These one-dimensional nanostructures exhibit exceptionally high mechanical strength but are extremely light-weight [5]. The incorporation of CNTs with metals, ceramics, and other insulators can further enhance the composites' mechanical, thermal, electrical, and magnetic properties [6–10].

Alumina (Al_2O_3) is a crystalline oxide of aluminum with high thermal conductivity but extremely low electrical conductivity [11]. Alumina nanoparticles are also attractive substrates due to their stability under high temperature and other rigorous processing conditions. Consequently, alumina finds application in zeolites, refractory polishers, and flame retardants [12–16]. The nanocomposite material created by combining CNTs with alumina is a promising material for its interesting magnetic properties as it encompasses traits of both its constituents. Therefore, it is desirable to create alumina composites with a uniform dispersion of CNTs to design hybrid materials with multiple benefits.

Kumari et al. reported on the thermal properties of CNT-alumina composites prepared by plasma sintering process [17]. Enhanced heat capacity, thermal diffusivity, and conductivity was achieved in samples treated to about 1500 °C. Siegel et al. reported on the CNT-alumina composites prepared by ultrasonic agitation in an ethanol mixture [18]. The fracture toughness increased by ~24% when CNTs were added in the alumina powders. Vermisoglou et al. studied the magnetic properties of aligned CNT arrays synthesized on Fe-catalyzed alumina oxide template [19]. These core-shell structures offered remarkable stability due to magnetic iron carbide particles' encapsulation by protective carbon shells and reduced interparticle magnetic coupling. Verma et al.

---

achieved a three-fold increase in the saturation magnetization of the CNT-cobalt ferrite by creating the nanocomposites [20]. The increased magnetic strength was attributed to the proximity effect between homogeneously distributed ferrites on the surface of carbon nanotubes. Yang et al. developed CNT reinforced aluminum hypophosphite composites with enhanced thermal stability, flame retardancy, and mechanical properties [21]. Detailed analysis showed that the incorporation of CNTs in the composites produced microspheres that could effectively reduce heat conduction during combustion.

There are many attempts to insert CNTs in these composite materials for various functionalities. Plasma sintering, ball-milling, and hydrothermal processes have been used in the past with various degrees of success regarding the homogeneity of CNTs [12,22,23]. High temperature (2000 °C) and physical treatment during the synthesis of CNTs can result in the damage or non-uniform dispersion of CNTs within alumina during these processes. The chemical vapor deposition (CVD) process is a promising method for directly assimilating CNTs in the composites at relatively low temperatures (800 °C) and normal atmospheric pressure. We aim to develop nanocomposites with tunable magnetic properties using the CVD process for various technological applications. This approach allows to overcome the low-yield, high-cost, and volatility of other methods and can be adapted to manufacture composite structures. This work presents a detailed study of CNT/Al_2O_3 nanocomposites prepared by the CVD process using iron as a catalyst. Iron nanoparticles dispersed in the alumina powder facilitated the precipitation of carbon atoms and resulted in the formation of tubular structures. The composites are characterized by X-ray diffraction studies (XRD), scanning electron microscopy (SEM), transmission electron microscopy (TEM), thermogravimetric analysis (TGA), Mössbauer spectroscopy, vibration sample magnetization (VSM), and field-cooled (FC) or zero-field-cooled (ZFC) magnetization measurements. As compared to the magnetization of 0.03 e.m.u./g at an applied field of 1.5 T for the Fe-catalyzed Al_2O_3, the saturation magnetization of CNT/Al_2O_3 is 1.78 e.m.u./g, which represents an increment of ~5800%. The coercivity of CNTs/Al_2O_3 composites increased from 0.036 T at 300 K to 0.285 T at 5 K. The possible explanations on the CNT facilitated enhancement in the magnetic properties of CNT-alumina nanocomposites are discussed.

2. Experimental method

2.1. Catalyst insertion

To disperse Fe catalyst seeds uniformly, alumina powder (2 g, Baikowski Inc, CR30F) was thoroughly mixed with 100 ml isopropyl alcohol (Sigma-Aldrich, 99.5%). Then, 0.1 g iron acetate tetrahydrate (Sigma-Aldrich, 95%) was dissolved into the mixture and sonicated for 1 h. The mixture was heated inside a box furnace at 120 °C for 24 h. The resulting dry powder was grounded into fine particles before inserting into a tube furnace.

2.2. Chemical vapor deposition

Fe-catalyzed Al_2O_3 powders were placed inside a tube furnace. The synthesis was carried in normal atmospheric pressure within an inert environment created by argon gas's continuous flow (100 sccm, 99.999%). The temperature of the furnace was increased to 800 °C at the rate of 50 °C/min. Upon stabilization, the hydrogen gas (100 sccm, 99.999%) was introduced in the chamber to reduce the catalyst for 30 min. After this step, acetylene (50 sccm, 99.6%) was used as a precursor for the deposition of CNTs for another 30 min. During this stage, the flow rates of Ar and H_2 gases were increased to 600 sccm and 400 sccm, respectively. After the completion of the synthesis, the sample was allowed to cool down slowly in the presence of an argon environment.

2.3. Material characterization

The samples' surface morphology was observed using a Hitachi 3400 N field emission SEM. TEM investigations were carried out using Technai Osiris, equipped with an energy dispersive X-ray (EDX) analyzer. The crystallinity of the sample was investigated by Rigaku miniflex X-ray diffractometer equipped with Cu-K_α radiation. The XRD patterns were collected with a step size of 0.05° and a 5°/min scan rate at 40 kV and 25 mA. TGA data were collected to determine the weight percent of CNTs in the composites using a TA Q500 instrument. Approximately 25 mg of the powdered sample was heated in an open platinum pan at 10 °C/min to measure the rate of mass loss as a function of temperature in the range of 20–1000 °C.

2.4. Mössbauer spectroscopy

Mössbauer spectroscopy was used to investigate the oxidation states and magnetic properties of iron in the Fe-catalyzed Al_2O_3 and CNT/Al_2O_3 composites. The measurements were performed using an MS4 spectrometer connected to a Janis cryostat, operating in the constant acceleration mode in transmission geometry. The Mössbauer spectroscopy measurements were performed at room temperature and cryogenic conditions (6 K).

2.5. Hysteresis measurements

The magnetic study was performed by a vibrating sample magnetometer (VSM) equipped with a 3-T electromagnet (Microsense Co.). ZFC and FC measurements were performed in a magnetic property measurement system (MPMS, Quantum Design) by lowering the temperature of the sample down to 5 K and with a magnetic field up to 2 T.

3. Results and discussion

3.1. Morphological analysis by transmission electron microscopy

During the CVD process for the synthesis of CNTs, the carbon precursor (C_2H_2) is dissociated into elemental carbon in an oxygen-free environment. Transition metal catalysts like iron, cobalt, and nickel help crystallize those carbon atoms to form tubular CNT structures. The observed morphology and structure of CNT/Al_2O_3 composites are shown in TEM images, Fig. 1. A representative low magnification image of Fig. 1 (a) shows the formation of hollow bamboo shaped CNTs dispersed in the matrix of Al_2O_3. The dark contrast at the tip of CNTs is from Fe-catalysts used during the CVD process. This shows that the CNTs follow the "tip-growth" model after the decomposition of acetylene [24]. During the annealing treatment, iron acetate reduces into metallic iron particles. These catalyst "seeds" serve as the sites for the dissolution and crystallization of carbon to produce graphitic tubular structures. As more and more carbon atoms are captured, the length of the CNTs increases with Fe-catalyst at the tip. The energy dispersive X-ray spectrometry (EDX) of the sample confirmed the presence of Al, O, Fe, and C in the composites, Fig. 1 (b). The additional contribution from copper in EDX spectrum is due to the copper grid used for mounting the sample. The elemental dispersive spectroscopy in Fig. 1(c–f) shows the homogeneous distribution of aluminum, oxygen, iron, and carbon throughout the composite.

3.2. Surface analysis by scanning electron microscopy

The SEM image of Fig. 2 (a) displays the morphologies of as-received alumina oxide particles. After the CVD process, the CNTs form a dense network of crosslinked fibers distributed throughout the composites, Fig. 2 (b). It is clearly seen that alumina oxide contains polydisperse particles (150 ±40) *nm* with sharp edges, (Fig. S1). The average diameter of CNTs is (40 ±10) *nm*, (Fig. S2). We expect these CNT/Al_2O_3
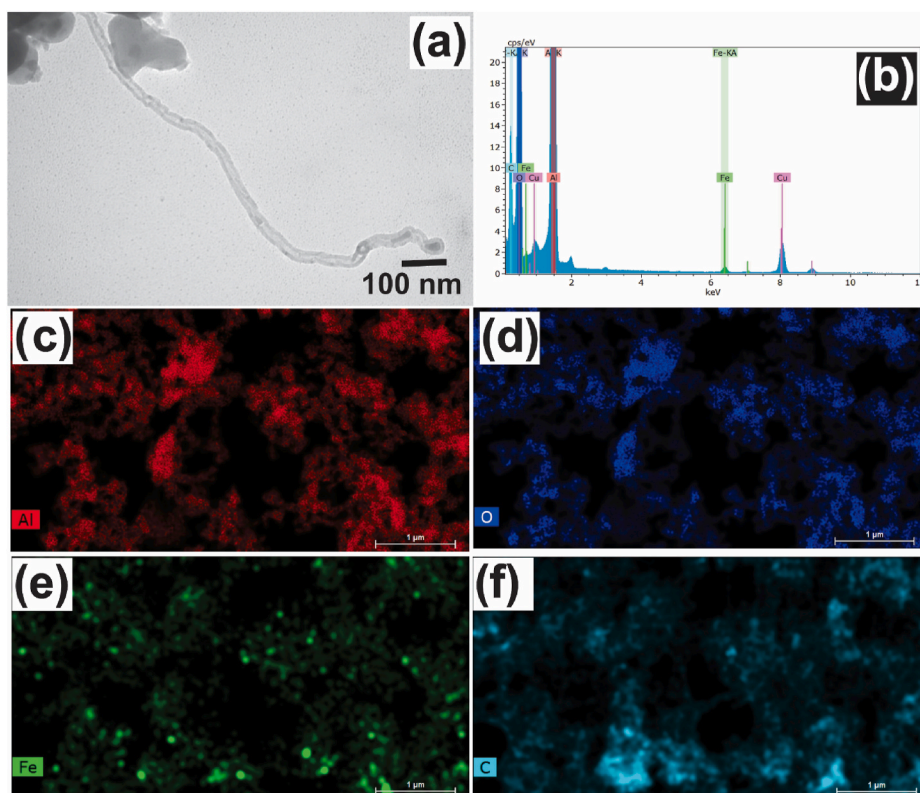
Fig. 1. (a) Transmission electron microscopic images of carbon nanotubes dispersed along with Al_2O_3 nanoparticles. (b) Energy-dispersive X-ray spectrometry analysis of CNT/Al_2O_3 (c–f) Elemental mapping of aluminum, oxygen, iron, and carbon, respectively.
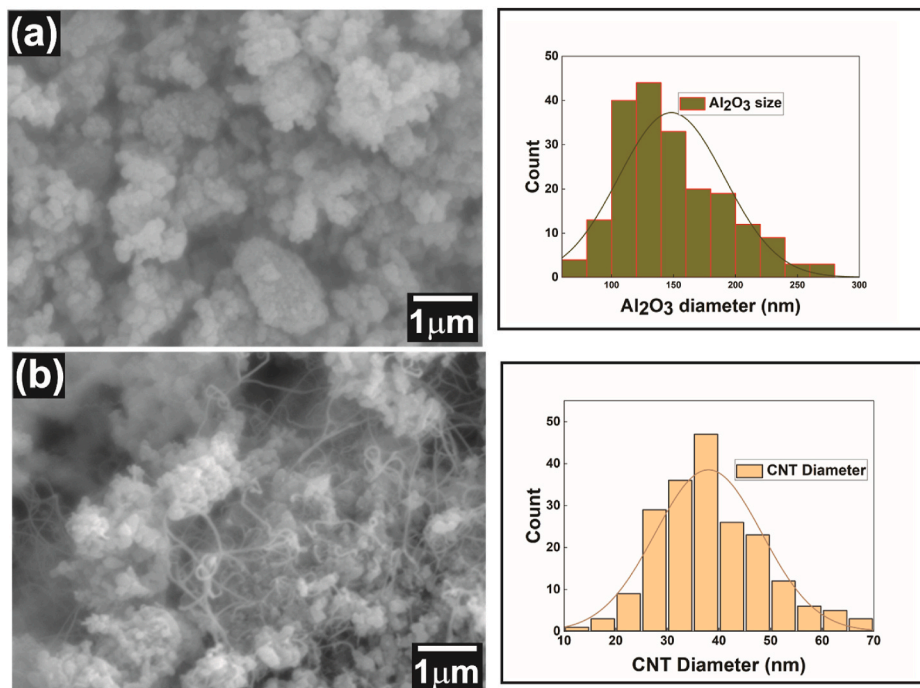

Fig. 2. Left panel: Scanning electron microscopic images of (a) Al_2O_3 nanoparticles (b) CNT/Al_2O_3 composites. The right panel are the size histograms of 200 individual particles determined using ImageJ software.

composites to exhibit enhanced mechanical, electrical, and thermal properties [8]. The histograms on the right panel of Fig. 2 show the particle size distribution of 200 aluminum oxide particles and carbon nanotubes determined using ImageJ software.

3.3. Structural analysis by X-ray diffraction studies

Fig. 3 shows the XRD patterns of pristine Al_2O_3, Fe-catalyzed Al_2O_3, and CNTs/Al_2O_3 composites, respectively. All the XRD patterns show
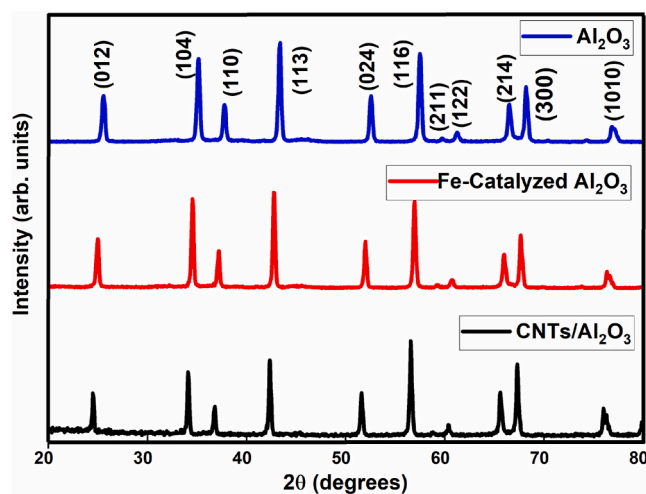
Fig. 3. X-ray diffraction profiles of (a) pristine Al_2O_3 (b) Fe-catalyzed Al_2O_3, (c) CNT/Al_2O_3 composites.

Fig. 4. Thermogravimetric analysis of CNT/Al_2O_3 nanocomposites.

sharply pronounced narrow peaks corresponding to the crystal structure of Al_2O_3 with no additional impurity phases. The diffraction peaks from (012), (104), (110), (113), (024), (116), (211), (122), (214), and (300) planes are obtained at 2θ values of 25.6°, 35.2°, 37.8°, 43.4°, 52.6°, 57.5°, 59.6°, 61.3°, 66.5°, and 68.2°, respectively. The powder X-ray diffraction peaks can be assigned to α-Al_2O_3 (JCPDS card No.71-1123). It should be noted that (002) and (100) peaks of graphite at 26° and 42° coincide with (012) and (113) peaks of alumina and cannot be distinguished. Also, the XRD profiles do not show any additional peaks from Fe catalyst because the proportion of iron salt to alumina powder is only 5% and the iron atoms contribute to around 1% of the weight of the composite. Nevertheless, the XRD peaks of CNT/Al_2O_3 reflect the crystallinity of composites after the vapor deposition process. The symmetry and narrowness of XRD peaks are indicative of the high crystallinity present in this sample. The crystallite size was calculated by using Scherer's equation: $t = \frac{0.89\lambda}{B \cos\theta}$, where t is crystallite size, λ is the wavelength of the X-ray, B is the full-width half maxima, and θ is the Bragg's angle [25]. The Al_2O_3 crystallite size determined using the most intense diffraction peak was about 40 nm. A careful investigation indicates that the XRD peaks shift minimally towards lower angles after the CVD process. This observation suggests that CNTs can absorb the strain induced during the volume expansion of Al_2O_3 because of their high modulus of elasticity.

3.4. Thermogravimetric analysis

TGA was performed to evaluate the amount of carbon in the composite after completing the CVD process. The thermal analysis of composites was carried from room temperature to 1000 °C, as shown in Fig. 4. In the first stage, a slow mass loss was observed between room temperature and 200 °C. The total weight loss of the sample was approximately 0.4 wt % during this phase because of the removal of atmospheric moisture collected by the sample during the handling process. The maximum weight loss from combustion occurred around 627 °C, corresponding to carbon dioxide and carbon monoxide production. The final residue appears like the alumina nanoparticles used at the beginning of the experiment. The amount of CNTs in the sample was about 7%, as determined by the weight changes. The differential weight change curve has a prominent peak at around 627 °C because of the combustion of CNTs in that temperature region [26].

3.5. Mössbauer spectroscopy

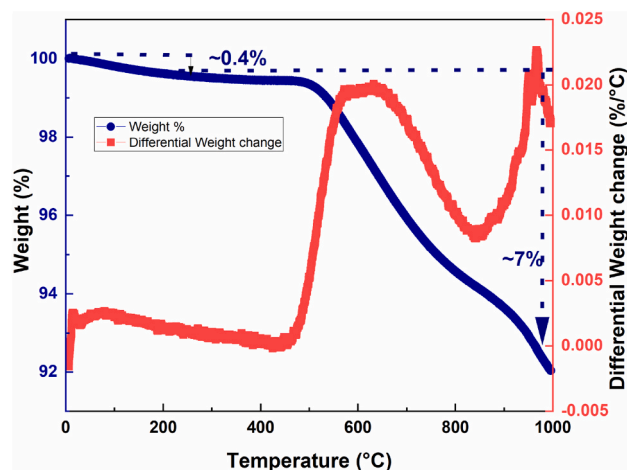Mössbauer spectroscopy provides quantitative information on the

oxidation state of Fe species, and it is a powerful tool to determine the contribution of Fe^{2+} and Fe^{3+} ions present in a sample. A 50 mCi ^{57}Co in Rh held at room temperature was used as a source. All centroid shifts-δ, are given with respect to metallic α−iron at room temperature. The spectra were least-square fitted using a Recoil software package (Ken Lagarec and Dennis Rancourt, 1998) to extract hyperfine parameters: centroid shifts (δ), quadrupole splitting (ΔE_Q), quadrupole shift (ε), magnetic hyperfine field (B_{hf}), Lorentzian linewidth (Γ), and intensities (I). Fig. 5 shows the spectra for Fe-catalyzed Al_2O_3 (left panel) and the CNT/Al_2O_3 composites (right panel).

Starting with the room-temperature spectrum for the Fe-catalyzed Al_2O_3 precursor, it has a relatively sharp two-line pattern, which is best fitted by two doublets with close-lying hyperfine parameters. These doublets have δ-values of 0.382 and 0.377 mm/s, and ΔE_Q of 0.478 and 0.759 mm/s, respectively. These values are characteristic values for high-spin Fe^{3+} in a superparamagnetic state [27,28]. As the temperature is lowered to 6 K, the spectrum is magnetically split, which can best be fitted with four sextets. The δ-values for all four sub-spectra are around 0.490 mm/s. The increase of the δ-values is in accordance with the second-order Doppler (SOD) shift, which is an increase of 0.06 mm/s for a 100 K decrease in temperature before saturation around 100 K. The B_{hf} value ranges from 49.5 T to 40.4 T for this sub-spectrum.

The room-temperature spectrum for the CNT/Al_2O_3 composites is best fitted with a singlet, a doublet, and three sextets (right column, top). The singlet has a δ-value of −0.105 mm/s resulting from Fe in austenite phase (face-centered-cubic) [29]. The doublet has a δ-value of 0.318 mm/s and a ΔE_Q value of 0.717 mm/s, which are characteristic values for small iron-oxide with high-spin Fe^{3+} in a superparamagnetic state. The first magnetic sub-spectrum, Q_3, with δ-value of -0.108 mm/s, having an intensity of 4%, is probably from Fe atoms in martensite phase [29]. The other two sextets, Q_4 and Q_5, with δ-values of 0.205 mm/s and 0.177 mm/s, and B_{hf} values of 20.8 T, and 20.0 T are signals from Fe_3C [30]. The 6 K spectrum for this sample is also fitted with the same number of the sub-spectra with slightly different intensities. The extracted Mössbauer parameters for both samples are summarized in Table 1.

3.6. Magnetic hysteresis

The magnetic properties of pristine Al_2O_3, Fe-catalyzed Al_2O_3, and CNT/Al_2O_3 nanocomposites were investigated at room temperature using a VSM with a maximum applied field of 1.5 T. Both pristine and Fe-catalyzed Al_2O_3 are non-magnetic and do not show any preferential attraction towards a permanent magnet. The CNT/Al_2O_3 nanocomposite is attracted strongly towards an external magnet, showing that it is possible to modulate magnetic properties of a ceramic by forming a
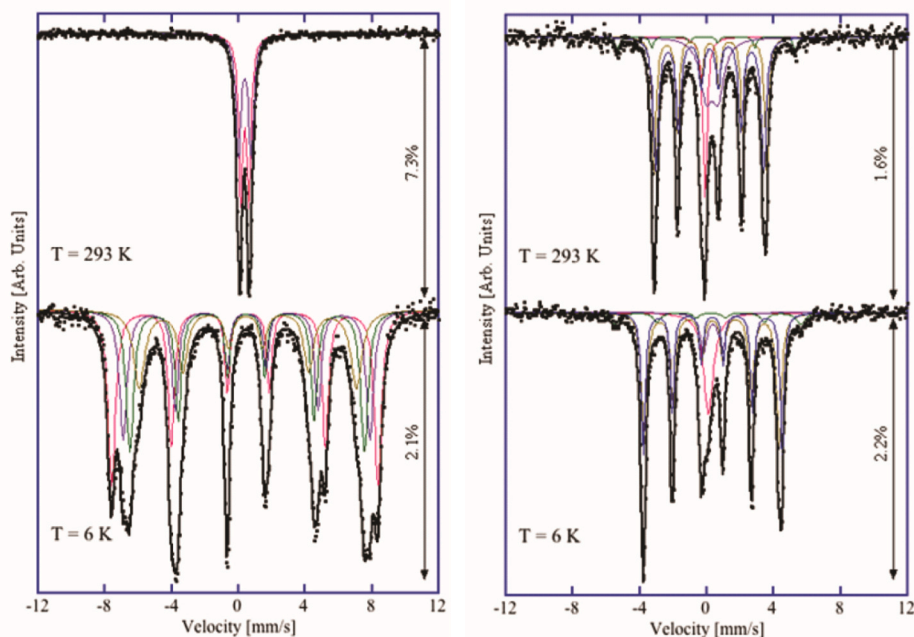
Fig. 5. Room-temperature and low-temperature Mössbauer spectra for the Fe-catalyzed Al_2O_3 precursor (left panel) and CNT/Al_2O_3 (right panel), at temperatures of 293 K and 6 K. The sub-spectra are also indicated.

Table 1
Summary of refined Mössbauer parameters for the used precursor and the Fe-based CNT sample measured at room temperature and 6 K: centroid shift-δ, magnetic hyperfine field, B_{hf}, quadrupole splitting/shift, $\Delta E_Q/\epsilon$, Lorentzian linewidth, Γ, and intensity, I. Estimated errors are in I $\pm 3\%$, in δ and ϵ ± 0.005 mm/s, in Γ ± 0.02 mm/s, and B_{hf} ± 0.5 T.

Components	Sample	Fe-catalyzed Al_2O_3		CNT/Al_2O_3	
	Temperature (K)	293 K	6 K	293	6
Q_1	δ_1 (mm/s)	0.382		−0.105	0.102
	$\Delta E_{Q,1}$ (mm/s)	0.478		–	–
	Γ_1 (mm/s)	0.31		0.29	0.72
	I_1 (%)	53		9	14
Q_2	δ_2 (mm/s)	0.377		0.318	0.367
	$\Delta E_{Q,2}$ (mm/s)	0.759		0.717	1.134
	Γ_2 (mm/s)	0.37		0.86	0.49
	I_2 (%)	47		18	8
Q_3	δ_3 (mm/s)		0.489	−0.108	0.161
	$B_{hf,3}$ (T)		49.5	33.0	34.3
	ϵ_3 (mm/s)		−0.105	0.088	−0.072
	Γ_3 (mm/s)		0.37	0.25	0.47
	I_3 (%)		30	4	6
Q_4	δ_4 (mm/s)		0.488	0.205	0.307
	$B_{hf,4}$ (T)		45.8	20.8	24.9
	ϵ_4 (mm/s)		−0.002	0.011	−0.021
	Γ_4 (mm/s)		0.39	0.25	0.35
	I_4 (%)		24	30	40
Q_5	δ_5 (mm/s)		0.492	0.177	0.342
	$B_{hf,5}$ (T)		43.6	20.0	25.7
	ϵ_5 (mm/s)		0.028	−0.001	0.012
	Γ_5 (mm/s)		0.39	0.34	0.26
	I_5 (%)		25	39	32
Q_6	δ_6 (mm/s)		0.493		
	$B_{hf,6}$ (T)		40.4		
	ϵ_6 (mm/s)		0.062		
	Γ_6 (mm/s)		0.57		
	I_6 (%)		21		

composite with CNTs. Fig. 6 (a) shows the typical hysteresis loops for different samples. The numerical values of saturation magnetization (M_s), remnant magnetization (M_r), and coercivity (H_c) obtained from these plots are listed in Table 1. Table 2 Initially, the pristine Al_2O_3 nanoparticles show the diamagnetic response with negligible coercivity

as evident by the straight-line graph with a negative slope. The hysteresis loop of Fe-catalyzed Al_2O_3 also shows a similar diamagnetic pattern due to significant contributions from alumina powder. The CNT/Al_2O_3 nanocomposites demonstrate a dramatic enhancement of ferromagnetic properties as evident from the sigmoidal hysteresis loop. When placed inside an increasing magnetic field, some or all of the atomic magnets in the nanocomposite tend to align with the applied magnetic field until the magnetic saturation (M_s) is achieved. When the magnetizing field is reduced, the magnetization decreases, lagging the applied field such that there is some residual magnetization (remanence) even when the applied magnetic field is reduced to zero. An additional magnetic force, H_c, is necessary to bring the magnetization to zero (see Fig. 6b). Compared to the magnetization of 0.03 e.m.u./g at an applied field of 1.5 T for the Fe-catalyzed Al_2O_3, the saturation magnetization of CNTs/ Al_2O_3 is 1.78 e.m.u./g, which represents an increment of ~5800%. Compared to M_s of ~210 e.m.u./g for the bulk iron, this saturation magnetization of 1.78 e.m.u./g is about 1% [31]. Since Fe atoms contribute to around 1%, by weight, in the composite, we can conclude that Fe atoms exist as alpha-Fe (ferromagnetic phase). The Fe-catalyzed Al_2O_3 sample showed near-zero coercivity, and the coercive field of nanocomposites increased significantly to 0.036 T when reinforced with CNTs suggesting that the magnetic "hardness" of the ceramic materials could be increased by the incorporation of CNTs during the synthesis. Kumar et al., measured the coercivities of crystalline Fe particles (5–9 nm) embedded on an amorphous Al_2O_3 matrices [32]. The coercivity of composites decreased from 0.01 T to 0.005 T as the Fe particle size decreases from 9 nm to 7 nm and, finally, the sample turns superparamagnetic when the Fe particle size becomes around 5 nm at 300 K. These results show that when the size of magnetic particles is reduced to few nanometers, they exhibit tunable physical temperature dependent properties such as high coercivities, giant magnetoresistance, superparamagnetism, and low saturation magnetization.

Fig. 7 (a) presents the magnetic hysteresis loops at room temperature (300 K) and under cryogenic conditions (5 K). Fig. 7 (a) clearly shows that the CNT/Al_2O_3 composites have vastly different coercivity values at different temperatures. The composites' coercivity increased from 0.036 T at 300 K to 0.285 T at 5 K. Hence, we can conclude that the CNT/ Al_2O_3 composites demonstrate "magnetically-hard" properties at lower
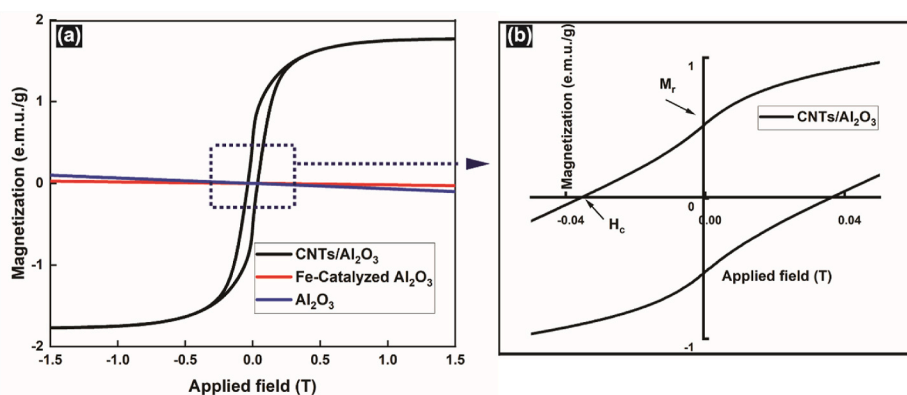
Fig. 6. (a) Room temperature magnetization (M) versus applied magnetic field (H) for pristine Al_2O_3, Fe-catalyzed Al2O3, and CNT/Al_2O_3 composites. (b) The enlarged view of the curve's section within the dotted rectangle of the M − H curve for CNT/Al_2O_3 composites.

Table 2

Values of coercive field (H_c), saturation magnetization (M_s), remnant magnetization (M_r), and squareness ratio (M_r/M_s) for pristine Al_2O_3, Fe-catalyzed Al_2O_3, and CNTs/Al_2O_3 nanocomposites.

	H_c (T)	M_s (e.m.u./g)	M_r (e.m.u./g)	Squareness ratio (M_r/M_s)
Al_2O_3	0	N/A	N/A	N/A
Fe-catalyzed Al_2O_3	0	0.03[a]	~0	~0
CNTs/Al_2O_3	0.036	1.78	0.53	0.30

[a] Unsaturated magnetization.

temperatures. The increase in coercivity at lower-temperatures can be ascribed to an increase in anisotropy upon cooling [33]. Furthermore, magnetic moments get "frozen" at lower temperatures, and the saturation magnetization is higher at the lower temperatures. At higher temperatures, the Brownian motion will disturb the magnetic moment vector's alignment towards the field direction, resulting in the decrease of the saturation magnetization.

The samples were first cooled, and then the temperature was raised steadily during FC and ZFC measurements. The FC and ZFC magnetization curves, Fig. 7 (b), indicate the splitting or bifurcation at temperatures below the room temperature. An external magnetic field of 0.01T, during FC measurements, aided magnetic moments' alignment and resulted in higher magnetization values. The ZFC curve is still very linear at 300 K, indicating the blocking temperature is above room temperature.
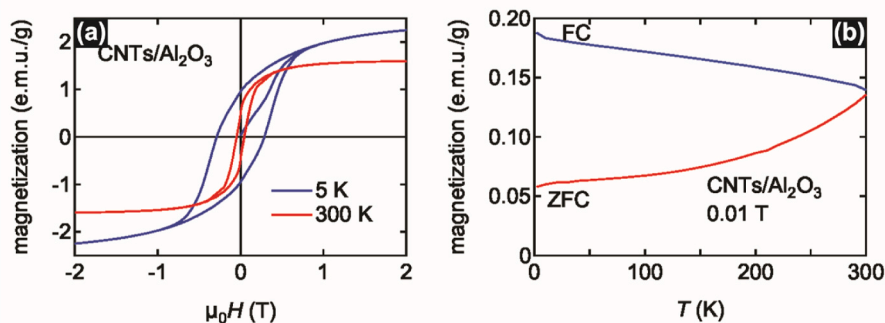
4. Conclusions

In conclusion, CNTs have been directly synthesized on Al_2O_3 nanoparticles to create a composite structure with superior magnetic properties. The diameter of CNTs is around 40 nm, and the weight of CNTs in the composite was around 7%. The iron catalysts used for the CVD process encapsulated within the CNTs are responsible for magnetic properties. The saturation magnetization of Fe-catalyzed Al_2O_3 increased by ~5800% after creating a composite with CNTs. The Al_2O_3 powders also underwent a magnetic hardening process with pronounced coercivity after the formation of composites. By using this approach, we achieved an eight-fold increment in coercivity of the composites at reduced temperatures. These composites can find application in three-dimensional magnetic circuits where the losses due to eddy currents are minimized due to insulation Al_2O_3 powder between conductive channels. Pellets of CNT/Al_2O_3 composites can withstand harsh corrosive environments and have potential for application as working electrodes during electrochemical measurements. Alternatively, when used as a fire retardant, the composite of Al_2O_3 with CNTs will have improved thermal performance since CNTs have excellent thermal transport properties.

CRediT authorship contribution statement

Steven Rhodes: Validation, Visualization, Writing – review &

Fig. 7. (a) Magnetization versus applied magnetic field curves taken at 5 K and 300 K. (b) Zero-field-cooled and field-cooled magnetization curves for CNTs/Al_2O_3 nanocomposites.

Declaration of competing interest

The authors declare that they have no known competing financial interests or personal relationships that could have appeared to influence the work reported in this paper.

Acknowledgments

Appendix A. Supplementary data

Supplementary data to this article can be found online at https://doi.org/10.1016/j.jpcs.2021.110455.

Data availability

The raw data required to produce these findings can be available from the corresponding authors.

References

[1] W.H. Shin, H.M. Jeong, B.G. Kim, J.K. Kang, J.W. Choi, Nitrogen-doped multiwall carbon nanotubes for lithium storage with extremely high capacity, Nano Lett 12 (2012) 2283–2288, https://doi.org/10.1021/nl3000908.

[2] Q. Cao, J.A. Rogers, Ultrathin films of single-walled carbon nanotubes for electronics and sensors: a review of fundamental and applied aspects, Adv. Mater. 21 (2009) 29–53, https://doi.org/10.1002/adma.200801995.

[3] V. Neves, E. Heister, S. Costa, C. Tîlmaciu, E. Flahaut, B. Soula, H.M. Coley, J. McFadden, S.R.P. Silva, Design of double-walled carbon nanotubes for biomedical applications, Nanotechnology 23 (2012) 365102, https://doi.org/10.1088/0957-4484/23/36/365102.

[4] M. Wang, Q. Yan, F. Xue, J. Zhang, J. Wang, Design and synthesis of carbon nanotubes/carbon fiber/reduced graphene oxide/MnO 2 flexible electrode material for supercapacitors, J. Phys. Chem. Solids 119 (2018) 29–35, https://doi.org/10.1016/j.jpcs.2018.03.029.

[5] M.M.J. Treacy, T.W. Ebbesen, J.M. Gibson, Exceptionally high Young's modulus observed for individual carbon nanotubes, Nature 381 (1996) 678–680, https://doi.org/10.1038/381678a0.

[6] D.-S. Lim, D.-H. You, H.-J. Choi, S.-H. Lim, H. Jang, Effect of CNT distribution on tribological behavior of alumina–CNT composites, Wear 259 (2005) 539–544, https://doi.org/10.1016/j.wear.2005.02.031.

[7] W.A. Curtin, B.W. Sheldon, CNT-reinforced ceramics and metals, Mater. Today. 7 (2004) 44–49, https://doi.org/10.1016/S1369-7021(04)00508-5.

[8] T. Zhang, L. Kumari, G.H. Du, W.Z. Li, Q.W. Wang, K. Balani, A. Agarwal, Mechanical properties of carbon nanotube–alumina nanocomposites synthesized by chemical vapor deposition and spark plasma sintering, Compos. Part Appl. Sci. Manuf. 40 (2009) 86–93, https://doi.org/10.1016/j.compositesa.2008.10.003.

[9] P. Bonnet, D. Sireude, B. Garnier, O. Chauvet, Thermal properties and percolation in carbon nanotube-polymer composites, Appl. Phys. Lett. 91 (2007) 201910, https://doi.org/10.1063/1.2813625.

[10] R. Yu, C.-F. Jiang, W. Chu, M.-F. Ran, W.-J. Sun, Decoration of CNTs' surface by Fe 3 O 4 nanoparticles: influence of ultrasonication time on the magnetic and structural properties, Chin. Chem. Lett. 28 (2017) 302–306, https://doi.org/10.1016/j.cclet.2016.07.014.

[11] G. Yamamoto, T. Hashi, Carbon nanotube reinforced alumina composite materials, in: N. Hu (Ed.), Compos. Their Prop, InTech, 2012, https://doi.org/10.5772/48667.

[12] A.K. Keshri, A. Agarwal, Splat morphology of plasma sprayed aluminum oxide reinforced with carbon nanotubes: a comparison between experiments and simulation, Surf. Coat. Technol. 206 (2011) 338–347, https://doi.org/10.1016/j.surfcoat.2011.07.025.

[13] D. Guaya, C. Valderrama, A. Farran, C. Armijos, J.L. Cortina, Simultaneous phosphate and ammonium removal from aqueous solution by a hydrated aluminum oxide modified natural zeolite, Chem. Eng. J. 271 (2015) 204–213, https://doi.org/10.1016/j.cej.2015.03.003.

[14] M.M.C. Chou, S.J. Huang, C.W.C. Hsu, Crystal growth and polishing method of lithium aluminum oxide crystal, J. Cryst. Growth. 303 (2007) 585–589, https://doi.org/10.1016/j.jcrysgro.2006.12.070.

[15] A. Ortiz, J.C. Alonso, V. Pankov, A. Huanosta, E. Andrade, Characterization of amorphous aluminum oxide films prepared by the pyrosol process, Thin Solid Films 368 (2000) 74–79, https://doi.org/10.1016/S0040-6090(00)00864-6.

[16] K. Balani, A. Agarwal, Wetting of carbon nanotubes by aluminum oxide, Nanotechnology 19 (2008) 165701, https://doi.org/10.1088/0957-4484/19/16/165701.

[17] L. Kumari, T. Zhang, G. Du, W. Li, Q. Wang, A. Datye, K. Wu, Thermal properties of CNT-Alumina nanocomposites, Compos. Sci. Technol. 68 (2008) 2178–2183, https://doi.org/10.1016/j.compscitech.2008.04.001.

[18] R.W. Siegel, S.K. Chang, B.J. Ash, J. Stone, P.M. Ajayan, R.W. Doremus, L. S. Schadler, Mechanical behavior of polymer and ceramic matrix nanocomposites, Scr. Mater. 44 (2001) 2061–2064, https://doi.org/10.1016/S1359-6462(01)00892-2.

[19] E.C. Vermisoglou, G.N. Karanikolos, G. Pilatos, E. Devlin, G.E. Romanos, C. U. Veziri, N.K. Kanellopoulos, Aligned carbon nanotubes with ferromagnetic behavior, Adv. Mater. 22 (2010) 473–477, https://doi.org/10.1002/adma.200901900.

[20] H. Verma, T. Mekuria, P. Seck, H. Hong, S.P. Karna, D. Seifu, Proximity effect tuned magnetic properties in composites of carbon nanotubes and nanoparticles of CoFe2O4, J. Magn. Magn. Mater. 501 (2020) 166438, https://doi.org/10.1016/j.jmmm.2020.166438.

[21] W. Yang, Z. Jia, Y. Chen, Y. Zhang, J. Si, H. Lu, B. Yang, Carbon nanotube reinforced polylactide/basalt fiber composites containing aluminium hypophosphite: thermal degradation, flame retardancy and mechanical properties, RSC Adv 5 (2015) 105869–105879, https://doi.org/10.1039/C5RA18606D.

[22] C.L. Xu, B.Q. Wei, R.Z. Ma, J. Liang, X.K. Ma, D.H. Wu, Fabrication of aluminum–carbon nanotube composites and their electrical properties, Carbon 37 (1999) 855–858, https://doi.org/10.1016/S0008-6223(98)00285-1.

[23] H. Barzegar-Bafrooei, T. Ebadzadeh, Synthesis of nanocomposite powders of γ-alumina-carbon nanotube by sol–gel method, Adv. Powder Technol. 22 (2011) 366–369, https://doi.org/10.1016/j.apt.2010.05.005.

[24] R. Purohit, K. Purohit, S. Rana, R.S. Rana, V. Patel, Carbon nanotubes and their growth methods, Procedia Mater. Sci. 6 (2014) 716–728, https://doi.org/10.1016/j.mspro.2014.07.088.

[25] A.W. Burton, K. Ong, T. Rea, I.Y. Chan, On the estimation of average crystallite size of zeolites from the Scherrer equation: a critical evaluation of its application to zeolites with one-dimensional pore systems, Microporous Mesoporous Mater 117 (2009) 75–90, https://doi.org/10.1016/j.micromeso.2008.06.010.

[26] D. Bom, R. Andrews, D. Jacques, J. Anthony, B. Chen, M.S. Meier, J.P. Selegue, Thermogravimetric analysis of the oxidation of multiwalled carbon nanotubes: evidence for the role of defect sites in carbon nanotube chemistry, Nano Lett 2 (2002) 615–619, https://doi.org/10.1021/nl0207297u.

[27] S. Kamali-M, T. Ericsson, R. Wäppling, Characterization of iron oxide nanoparticles by Mössbauer spectroscopy, Thin Solid Films 515 (2006) 721–723, https://doi.org/10.1016/j.tsf.2005.12.180.

[28] L. Häggström, S. Kamali, T. Ericsson, P. Nordblad, A. Ahniyaz, L. Bergström, Mössbauer and magnetization studies of iron oxide nanocrystals, Hyperfine Interact 183 (2008) 49–53, https://doi.org/10.1007/s10751-008-9750-5.

[29] A. Aydin, E. Guler, H. Aktas, H. Gungunes, Mössbauer studies on athermal martensite formation in an fe-ni-mn alloy, Bull. Mater. Sci. 25 (2002) 359–360, https://doi.org/10.1007/BF02708009.

[30] B. David, O. Schneeweiss, F. Dumitrache, C. Fleaca, R. Alexandrescu, I. Morjan, Powders with superparamagnetic Fe 3 C particles studied with Mössbauer spectrometry, J. Phys. Conf. Ser. 217 (2010) 012097, https://doi.org/10.1088/1742-6596/217/1/012097.

[31] S. Karmakar, S.M. Sharma, M.D. Mukadam, S.M. Yusuf, A.K. Sood, Magnetic behavior of iron-filled multiwalled carbon nanotubes, J. Appl. Phys. 97 (2005), 054306, https://doi.org/10.1063/1.1858878.

[32] D. Kumar, J. Narayan, A.V. Kvit, A.K. Sharma, J. Sankar, High coercivity and superparamagnetic behavior of nanocrystalline iron particles in alumina matrix, J. Magn. Magn. Mater. 232 (2001) 161–167, https://doi.org/10.1016/S0304-8853(01)00191-3.

[33] I. Ahamed, R. Pathak, R. Skomski, A. Kashyap, Magnetocrystalline anisotropy of ε -Fe 2 O 3, AIP Adv 8 (2018), 055815, https://doi.org/10.1063/1.5007659.